Using saturated absorption for super-resolution laser scanning transmission microscopy

Kentaro Nishida[1,2,a], Hikaru Sato[2,a], Ryosuke Oketani[2], Kentaro Mochizuki[3], Kenta Temma[1,2], Yasuaki Kumamoto[2], Hideo Tanaka[3] and Katsumasa Fujita[1,2,*]

[1] AIST-Osaka University Advanced Photonics and Biosensing Open Innovation Laboratory, AIST, 2-1 Yamadaoka, Suita, Osaka 565-0871, Japan

[2] Department of Applied Physics, Osaka University, 2-1 Yamadaoka, Suita, Osaka 565-0871, Japan

[3] Department of Pathology and Cell Regulation, Graduate School of Medical Sciences, Kyoto Prefectural University of Medicine, 465 Kajiicho, Kawaramachi-Hirokoji, Kamigyo, Kyoto, Kyoto 602-8566, Japan

[a] These authors contributed equally.

[*] Corresponding author: Katsumasa Fujita (**fujita@ap.eng.osaka-u.ac.jp**)

Abstract:

We improved the three-dimensional spatial resolution of laser scanning transmission microscopy by exploiting the saturated absorption of dye molecules. The saturated absorption is induced by the high-intensity light irradiation and localizes the signal within the centre of the focal spot. Our numerical calculation indicates that the spatial resolution in transmission imaging is significantly improved for both lateral and axial directions using nonlinear transmitted signals induced by saturated absorption. We experimentally demonstrated the improvement of the three-dimensional resolution by observing fine structures of stained rat kidney tissues, which were not able to be visualised by conventional laser scanning transmission microscopy.

Keywords (6): super-resolution microscopy, transmission microscopy, saturable absorption, optical sectioning, nonlinear microscopy, tissue imaging

Introduction

Confocal laser scanning microscopy[1–3] is capable of visualizing three-dimensional structures in a non-contact manner and is a powerful tool, especially for the observation of biological samples. This modality has a wide range of applications, as is capable of utilizing various types of optical responses of a sample as signals: reflection confocal microscopy visualizes surface structures of a sample with depth discrimination capability[4,5], and fluorescence confocal microscopy allows high-contrast volumetric imaging of molecules and organelles in a biological sample stained with fluorescent labels[6–9]. However, light absorption has not been directly utilized as a contrast mechanism in confocal microscopy because the spatial frequency information on the optical axis is not transferred in the optical system in transmission imaging[10].

Since the confocal pinhole cannot provide the axial resolution in absorption contrast, different approaches have been examined to image the three-dimensional distribution of light absorbers. In these attempts, the nonlinear absorption effects of contrast probes, such as two-photon absorption[11,12] and transient absorption[13–15] have been utilized. The nonlinear absorption effect is induced at the region where the photon density is high and can be utilized to localize the signal within the centre of the focal spot[16,17]. A technique for efficient detection of two-photon absorption by utilizing the

55 quadric dependence of the absorbed intensity to the excitation intensity[11] was used to
56 demonstrate volumetric absorption imaging of melanin[16] and red blood cells[18]. The use
57 of transient absorption can exploit the fact that the generation of transient absorption is
58 limited at the region where two-colour excitation beams are spatially overlapped[13].
59 Transient absorption microscopy is used as an effective method to investigate the three-
60 dimensional distribution of low-fluorescence material[14,15]. As a similar approach, the use
61 of optical effect following light absorption, such as photothermal effect[19,20], stimulated
62 emission[21], can also realize the three-dimensional resolution using absorption contrast.

63 In this paper, we exploited the saturated absorption of dye molecules to improve
64 the three-dimensional spatial resolution of laser scanning transmission microscopy.
65 Saturated absorption can be induced by high-intensity light irradiation as it saturates the
66 number of molecules at the excited state due to its non-zero lifetime[22,23]. Similar to other
67 nonlinear absorption effects, saturated absorption can occur only at the centre of the focal
68 spot and enables the observation of the three-dimensional distribution of light absorbers[24].
69 On the other hand, in our saturated-absorption transmission (SAT) microscopy, we
70 demonstrate the measurement of saturated absorption directly by detecting the light
71 transmitted through a sample, which can be realized using a conventional laser scanning
72 microscopy. We conducted a theoretical study of the optical process based on a two-level

73 energy diagram to show that absorption of dye molecules can be saturated, and the
74 saturated absorption signal can be efficiently extracted by the harmonic demodulation
75 technique[25,26]. Our calculation confirmed that the image size of a single point absorber
76 was significantly reduced by extracting the saturated absorption signal, which indicates
77 the improvement of spatial resolution due to nonlinear absorption. We also
78 experimentally obtained in-plane and cross-sectional images of stained rat kidney tissue
79 by using our proposed technique and demonstrated the improvement of spatial resolution
80 in both lateral and axial directions. Transmission microscopy is widely used as a standard
81 tool for observing dye-stained pathological sections for medical diagnosis. The
82 improvement of the spatial resolution in transmission imaging would contribute to finding
83 out small lesions in the pathological tissues, which conventional bright-field microscopy
84 cannot visualise.
85
86 **Two-level kinetic model for calculating saturable absorption of dye molecules**
87 To calculate the relationship between absorbed light power by a single dye molecule and
88 excitation intensity, we used a two-level kinetic model composed of the ground state and
89 the excited state, as shown in Figure 1(A). S_0 and S_1 represent the existence probability
90 of a molecule in the ground state and the excited state, respectively. k_{ex} [s^{-1}], k_f [s^{-1}], k_{nf} [s^{-}

91 [1], and k_{st} [s^{-1}] represent the rate constants for excitation, spontaneous fluorescence

92 emission, spontaneous non-fluorescence relaxation, and stimulated emission, respectively.

93 By using these constants, we can represent the rate equation for S_1 as follows:

94 $$\frac{dS_1}{dt} = -(k_f + k_{nf} + k_{st})S_1 + k_{ex}S_0 \quad (1)$$

95 $$S_1 + S_0 = 1 \quad (2)$$

96 Defining S as

97 $$S = S_0 - S_1 \quad (3),$$

98 Eq. (1) and Eq. (2) are reduced to a single differential equation as follows:

99 $$\frac{dS}{dt} = -(k_f + k_{nf} + k_{st} + k_{ex})S + (k_f + k_{nf} + k_{st} - k_{ex}) \quad (4)$$

100 When we assume a steady state,

101 $$\frac{dS}{dt} = 0 \quad (5)$$

102 Thus, from Eq. (4) and Eq. (5), we get

103 $$S = \frac{(k_f + k_{nf} + k_{st} - k_{ex})}{(k_f + k_{nf} + k_{st} + k_{ex})} \quad (6)$$

104 Here, we can express the rate coefficients of k_{ex} and k_{st} as follows:

105 $$k_{ex} = k_{st} = \frac{\sigma\lambda I}{hc} \quad (7)$$

106 where σ [cm^2] is the absorption cross-section of a dye molecule, I [W/cm^2] is the intensity

107 of incident light, λ [cm] is excitation wavelength, h [J s] is the Planck constant, and c

108 [cm/s] is the speed of light in vacuum. By substituting Eq. (7) into Eq. (6), we get

$$S = \frac{1}{\frac{I}{I_S} + 1} \quad (8)$$

where

$$I_S = \frac{hc}{2\sigma\lambda}(k_f + k_{nf}) \quad (9)$$

is termed saturation intensity [W/cm^2], which depends on the photophysical parameters of the dye molecule and the wavelength of the incident light. P_{ab} [W] the absorbed power by the molecule is given by

$$P_{ab} = (\frac{hc}{\lambda})k_{ex}S = \frac{\sigma I}{\frac{I}{I_S} + 1} \quad (10)$$

By using Eq. (10), we plot the relationship between excitation intensity and absorbed power by a single dye molecule in Figure 1(B). For the calculation, we used the photophysical parameters of eosin Y reported by Jones et al[27]. We used the excitation wavelength of 532 nm, which is located on the absorption peak of eosin Y[28]. At the low excitation intensity region of ~ 10^3 W/cm^2, the absorbed power by a molecule was linearly increased with the excitation intensity. However, as the excitation intensity increased further, the absorbed power by a molecule started to deviate from the linear trend and finally became saturated.

By using P_{ab}, transmitted intensity through the molecule, I_{tr} [W/cm^2], is calculated as follows:

$$I_{tr} = I - \frac{P_{ab}}{A} = (1 - \frac{\sigma}{A(\frac{I}{I_S} + 1)})I \quad (11)$$

where A [cm^2] is the area of the incident light. We can extract the nonlinear components in the detected transmitted signal by the harmonic demodulation technique[25]. In this technique, the nonlinear signal is extracted by applying temporal modulation at a single frequency to excitation intensity and demodulating the harmonics signal generated due to the nonlinear relationship between signal and excitation intensity. We applied a modulation frequency of 10 kHz to excitation intensity in this study.

Figure 1(C) shows the calculated relationship between excitation intensity and the demodulated transmitted signal from a single eosin Y molecule at the fundamental frequency (f = 10 kHz), 2nd order harmonic frequency ($2f$ = 20 kHz), and 3rd order harmonic frequency ($3f$ = 30 kHz), respectively. In Figure 1(C), the signal demodulated at f linearly increases with the excitation intensity, indicating the detection of linear components in the transmitted signal. On the other hand, the signals demodulated at $2f$ and $3f$ show an increase with the 2nd and 3rd order nonlinearities, respectively. This calculation result confirms that the nonlinear components included in transmitted signals are able to be extracted by demodulating at the harmonic frequencies. The order of the nonlinearity of the demodulated signals corresponds to the order of demodulation frequency at low excitation intensities. However, when the excitation intensity is

144 increased, the signals demodulated at 2*f* and 3*f* deviate from the 2nd order and 3rd order
145 slope respectively, and finally showed saturations.

146 We confirmed the improvement of the three-dimensional spatial resolution in our
147 technique by numerical calculations. We calculated the images of a single point absorber
148 reconstructed by the demodulated signals and evaluated the spatial resolutions by
149 measuring the image size. Note that the calculation result does not correspond to the point
150 spread function used for fluorescence imaging because the transmission image is not
151 simply formed by the linear combinations of signals at each point within the excitation
152 spot, which is due to the coherent nature of the transmitted light through the sample.

153 Figure 2(A) shows the calculated intensity distribution of the excitation focal
154 spot. The excitation wavelength was 532 nm, and the numerical aperture (NA) of the
155 objective lens was 1.40 in this calculation. Figure 2(B) shows the image of a single point
156 absorber reconstructed by the signal demodulated at *f*, which corresponds to the inversion
157 of the intensity distribution at the excitation focal spot shown in Figure 2(A). Figures 2(C)
158 and 2(E) are the images of a single point absorber reconstructed by the signal
159 demodulated at 2*f* and 3*f*, respectively. In Figures 2(C) and 2(E), the signal intensities
160 from the absorber are higher than the background level because the images were
161 reconstructed by the nonlinear components in the transmitted signals generated from the

absorber. To compare the spatial resolution of these images in negative contrast, we calculated the inverted images of Figures 2(C) and 2(E) as shown in Figures 2(D) and 2(F), respectively. We compared the line profiles of Figures 2(B), 2(D), and 2(F) in the lateral direction in Figure 2(G). Full widths at half maximum (FWHMs) of Figures 2(B), 2(D), and 2(F) are 174 nm, 130 nm, and 109 nm in the lateral direction, respectively. The image sizes are reduced by factors of 1.34 and 1.60 by demodulating the 2^{nd} order and 3^{rd} order of nonlinear signals because of the improvements of spatial resolution. We also obtained the line profiles in the axial direction in Figure 2(H). The FWHMs in the axial direction are 497 nm, 346 nm, and 288 nm for Figures 2(B), 2(D), and 2(F), showing the reduction of the image sizes at the by factors of 1.44 and 1.73 for 2(D) and 2(F), respectively. These results confirm that our technique can improve the three-dimensional spatial resolution of the image.

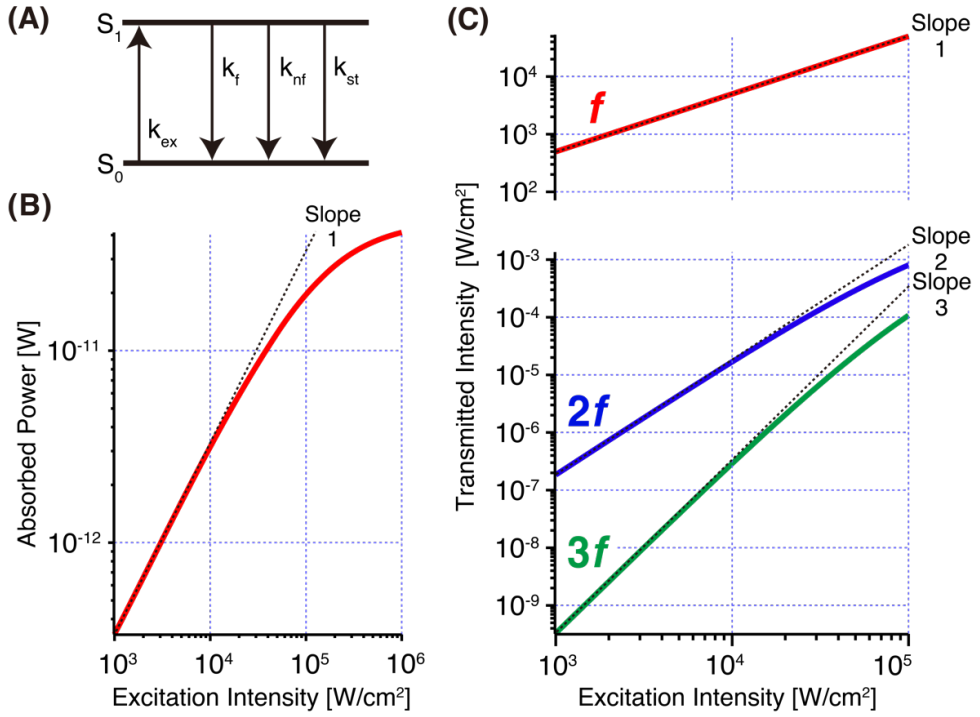

177

178 Fig. 1. (A) Schematic of the two-level kinetic model. S_0 and S_1 represent the existence

179 probability of molecules in the ground state and the excited state, respectively. k_{ex} [s^{-1}], k_f

180 [s^{-1}], k_{nf} [s^{-1}] and k_{st} [s^{-1}] represent the rate constants for excitation, spontaneous

181 fluorescence emission, spontaneous non-fluorescence relaxation and stimulated emission,

182 respectively. (B) Relationship between excitation intensity and absorbed light power by

183 a single eosin Y molecule, calculated by a two-level kinetic model. The excitation

184 wavelength was 532 nm. (C) Calculated relationships between excitation intensity and

185 demodulated transmitted signal intensities from a single eosin Y molecule at the

186 fundamental frequency (f=10kHz), 2nd harmonic frequency ($2f$), and 3rd harmonic

187 frequency ($3f$). The modulation frequency of excitation intensity was 10 kHz. The beam

188 size was 1.6×10^{-9} cm^2 in the calculation.

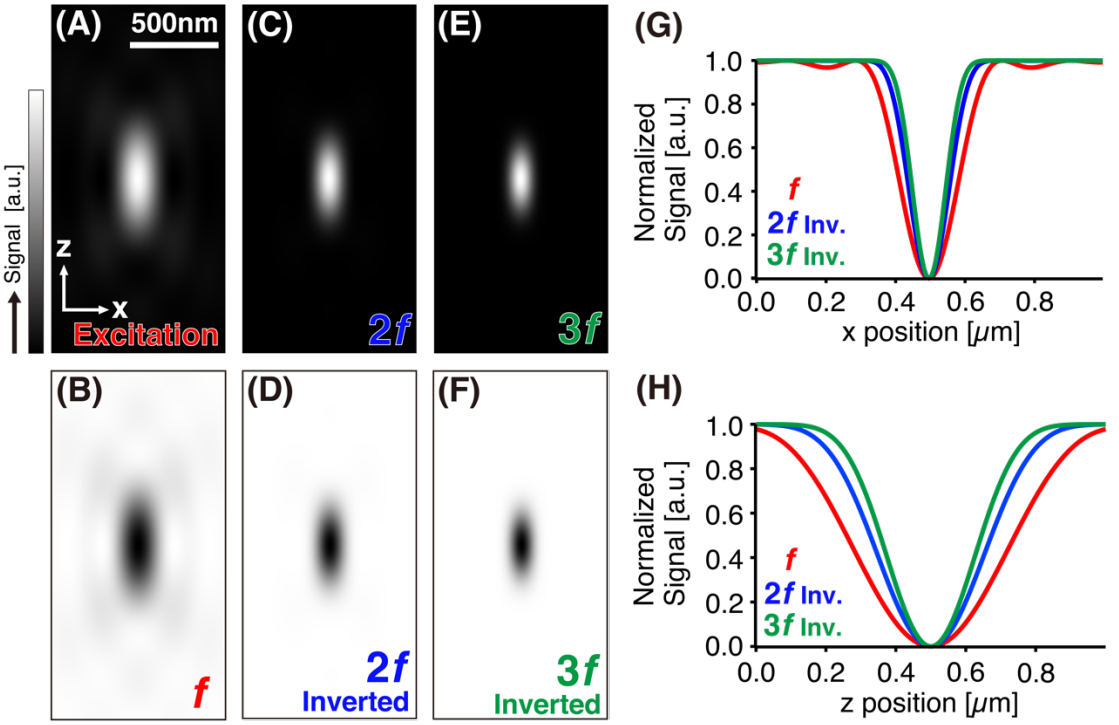

189

190 Fig 2. (A) Calculated intensity distribution of the excitation focal spot. The excitation

191 wavelength was 532 nm. The NA of the objective lens for excitation was 1.40. The

192 direction of linear polarization was y-direction. (B, C, E) Calculated images of a single

193 point absorber, reconstructed by the signal demodulated at f (B), $2f$ (C), and $3f$ (E),

194 respectively. The photophysical parameters of eosin Y were used for the calculation. The

195 excitation intensities were 10^2 W/cm^2 (B), 10^3 W/cm^2 (C), and 10^4 W/cm^2 (E). (D, F)

196 Inverted images of (C) and (E), respectively. (G, H) Line profiles of (B), (D), and (F)

197 obtained along x-direction (G) and z-direction (H), respectively.

198

199

We also theoretically investigated the dependence of nonlinear absorption signals on the dye concentration and the sample thickness. Basically, the nonlinear absorption signal proportionally increases as the number of molecules increases. However, if the dye concentration or the sample thickness is increased, nonlinear signals decrease because the amount of detectable transmitted signal becomes small, which makes the interpretation of the resultant image difficult. To avoid this situation, the ranges of dye concentration and the sample thickness available in our technique was investigated.

When the incident light is transmitting in a thick sample, the reduction of incident light intensity dI [W/cm^2] after traveling through a sample with a thickness of dz [cm] is expressed as follows:

$$dI = -\alpha(I(z))I(z)dz \quad (12)$$

where α is termed the absorption coefficient. The absorption coefficient is proportional to S, and it is given by

$$\alpha(I(z)) = \alpha_0 S = \frac{\alpha_0}{\frac{I(z)}{I_S} + 1} \quad (13)$$

where

$$\alpha_0 = N_A C \sigma \quad (14)$$

is the absorption coefficient when the intensity of incident light is zero ($I = 0$). N_A [mol^{-1}] is Avogadro's constant. C [mol/cm^3] is the concentration of molecules. We solved the

differential equation Eq. (12) to get

$$I_{tr} = I_S W_0(g(I_{ex})) \quad (15)$$

$$g(I_{ex}) = \frac{I_{ex}}{I_S}\exp(\frac{I_{ex}}{I_S})\exp(-N_A\sigma CL) \quad (16)$$

where I_{ex} [W/cm^2] is the intensity of illumination light to the sample, I_{tr} [W/cm^2] is the intensity of transmitted light passed through the sample, L[cm] is the thickness of the sample, and W_0 (x) represents the Lambert W function, which is the inverse function of $y = x\exp(x)$.

By using Eq. (15) and Eq. (16), we calculated the dependence of the demodulated transmitted signal intensity on the thickness and the concentration of the sample, as shown in Figures 3(A-C). The thickness and the concentration of the sample were expressed by using the column density, CL [mol/cm^2], which is the product of the concentration of molecules, C [mol/cm^3], and the thickness, L [cm]. In this calculation, we assumed that the thickness of the sample is smaller than the depth of the focus, and the beam size does not change during propagation at the beam waist. Although the above assumption is not always satisfied in practical situations, this simple model is still helpful for us to understand the difference of image contrast between the linear and the nonlinear transmission images shown in the sections below. The calculations were performed for excitation intensities of 10^2 W/cm^2, 10^3 W/cm^2, 10^4 W/cm^2, and 10^5 W/cm^2, respectively.

In Figures 3(A-C), the transmitted signals demodulated at f always decreases with the increase of the column density, indicating that the amount of the linear transmitted signal corresponding with the absorption of the sample. On the other hand, the signals demodulated at $2f$ increase at the column density lower than ~4.0×10^{-9} mol/cm^2, where the nonlinear components in the transmitted signal increase with the number of dye molecules. However, at the column density higher than ~4.0×10^{-9} mol/cm^2, the intensities of the signals demodulated at $2f$ decrease with the increases of the column density. In this region of column density, the transmitted light becomes small due to the strong light absorption in the sample, and the amount of detected nonlinear signal also becomes small. Then, the amounts of the signals demodulated at $2f$ no longer represent the number of absorbers unambiguously. Our calculation indicates that the product of the concentration of eosin Y and the thickness should be adjusted below 4.0×10^{-9} mol/cm^2 in sample preparation. The signal demodulated at $3f$ also shows such a decrease when the column density is larger than ~4.0×10^{-9} mol/cm^2, showing similarity to the case of the signal demodulated at $2f$.

The graphs of the signals demodulated at $3f$ showed the dips in signal intensity at the column density of 5.0×10^{-9} mol/cm^2, which is caused by the phase inversion of the nonlinear transmitted signal at this point. Since the phase of the modulated nonlinear

signal depends on the relationship between the illumination and transmission intensities, the sign of the demodulated signal can be positive, negative, or zero depending on the modulation range of excitation intensity and the sample property. In our calculation, the nonlinear signal also showed zero value, and the phase inversion was observed around this point, which produced the dip in the log plot. The same behavior of the demodulated nonlinear signals was observed in the investigation of scattering saturation[29].

The above calculation helps understand the image contrast of SAT microscopy, which depends on the sample thickness and dye concentration. However, the above interpretations are valid only when the sample thickness is smaller than the depth of the focus. We need a different model for a thicker sample and a consideration of the linear attenuation during propagation through the out-of-focus planes. In this research, we focused on investigating the light absorption at the focal position using a thin-sample model to understand the contrast mechanism provided by saturated absorption.

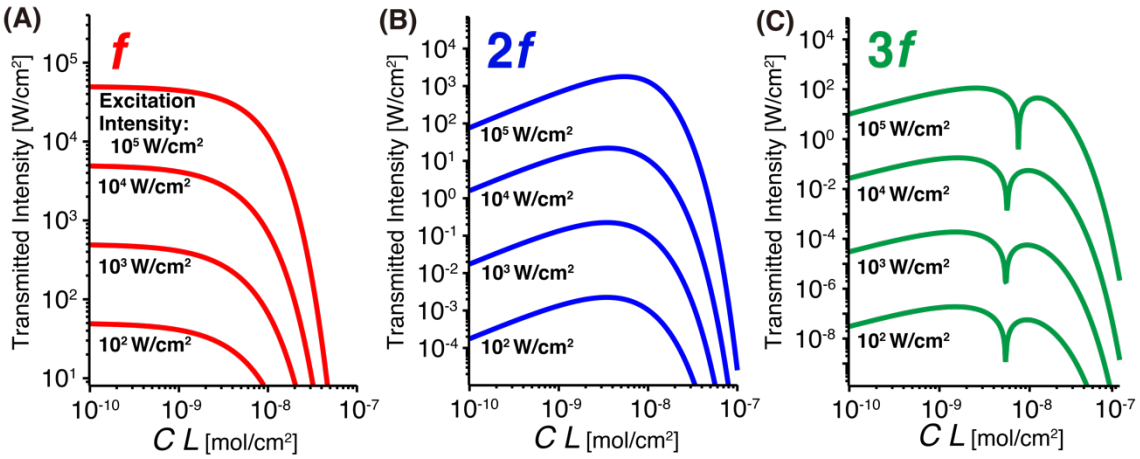

Fig. 3. (A-C) Dependence of the demodulated transmitted intensities on the column density [mol/cm^2], which is the product of the concentration of eosin Y molecule (C [mol/cm^3]) and the thickness (L [cm]). The demodulation frequencies were f (A), $2f$ (B), and $3f$ (C), respectively. Excitation intensities were 10^2 W/cm^2, 10^3 W/cm^2, 10^4 W/cm^2 and 10^5 W/cm^2.

Experimental measurement of the nonlinear transmitted signal from eosin Y

We experimentally measured the nonlinear transmitted signal generated from eosin Y solution by using the optical setup of SAT microscopy. Figure 4 shows the experimentally measured relationship between excitation intensity and demodulated transmitted signal intensity through eosin Y solution at the fundamental frequency (f) and 2nd harmonic frequency ($2f$), respectively. The signal demodulated at f shows the linear relation to the

282 excitation intensity, although the signal intensity starts exceeding from the linear trend
283 due to the saturation of absorption as the excitation intensity is increased. On the other
284 hand, the signal demodulated at $2f$ shows 2^{nd} order nonlinear relations when excitation
285 intensity is higher than ~1.0 $\times 10^4$ W/cm^2. The 2^{nd} order nonlinear component appears
286 only when the amounts of the nonlinear signals are larger than the shot noise of
287 transmitted light at the detector. Therefore, at the low excitation intensity region below
288 ~1.0 $\times 10^4$ W/cm^2, the signal demodulated at $2f$ increases following the square root of
289 excitation intensity, instead of following the 2^{nd} order slope. The intensity ratio of 2^{nd}
290 order nonlinear signal is about 3.2% to the linear signal at the excitation intensity of ~10^4
291 W/cm^2, in this measurement using the solution. This ratio is ~10^7 times higher than the
292 value shown in our theoretical calculation for a single molecule (Figure1(C)), indicating
293 the amount of nonlinear signal strongly depends on the number of the molecules in the
294 sample. This experimental result confirms that the absorption of eosin Y is saturable at
295 high excitation intensity, and the produced nonlinear components of the transmitted signal
296 are extracted by harmonic demodulation. In this experiment, we were not able to detect
297 3^{rd} order nonlinear components in the transmitted signal, due to the small amount of the
298 3^{rd} order nonlinear signal.

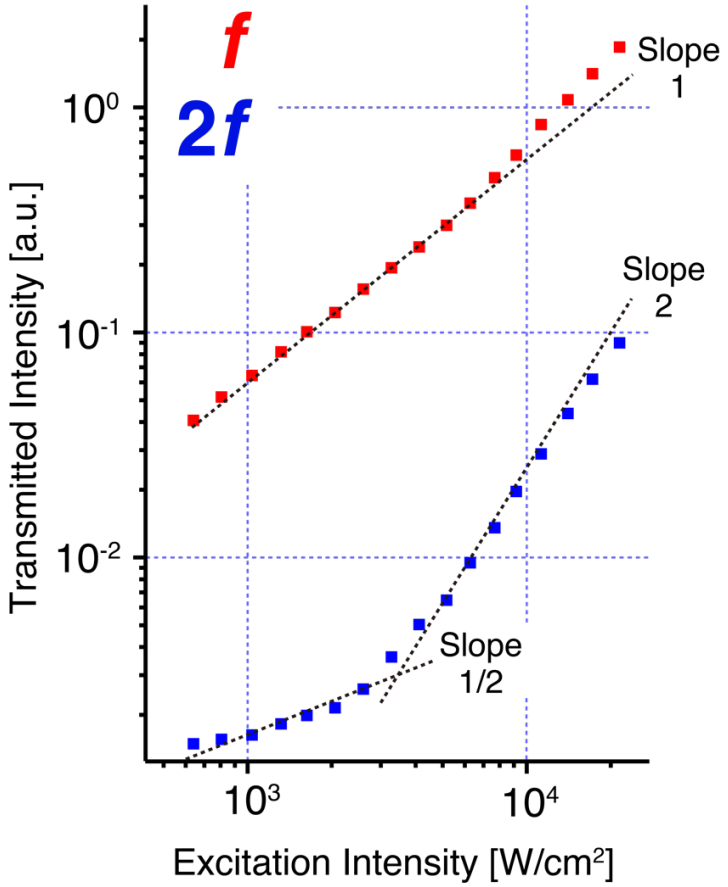

Fig. 4. Experimentally measured relationship between excitation intensity and intensity of the demodulated transmitted signal from eosin Y solution at the fundamental frequency (f=10kHz) and 2nd harmonic frequency ($2f$). The modulation frequency of the excitation intensity was 10kHz. The excitation wavelength was 532 nm.

Imaging of stained polystyrene microbeads

We obtained images of polystyrene microbeads stained with eosin Y by using SAT microscopy to confirm the improvement of spatial resolution. Figures 5(A) and 5(B) show the transmission images of single polystyrene microbeads, reconstructed by the signal

demodulated at f and $2f$, respectively. The diameter of polystyrene microbeads was 2 μm. In Figure 5(C), we compared the line profile of the transmission image of the microbead indicated by white arrowheads in Figures 5(A) and 5(B). Figure 5(C) shows that the spread of the image reduces in Figure 5(B) compared to Figure 5(A) and indicates the improvement of spatial resolution by reconstructing the image with the nonlinear signal. To evaluate the improvement of spatial resolution, we measured the full widths at half maximums (FWHM) of signal profiles for five polystyrene microbead images. The averaged FWHM values were 2.9 ± 0.11 and 2.1 ± 0.19 μm for linear image and 2^{nd} order nonlinear image, respectively, which confirmed the improvement of the spatial resolution in SAT imaging. We also obtained the images of two closely located microbeads in Figures 5(D) and 5(E) to confirm the improvement of two-point spatial resolution. In Figure 5(F), we compared the line profile of Figures 5(D) and 5(E). In the nonlinear image, we can resolve two microbeads with the improvement of two-point spatial resolution in SAT microscopy.

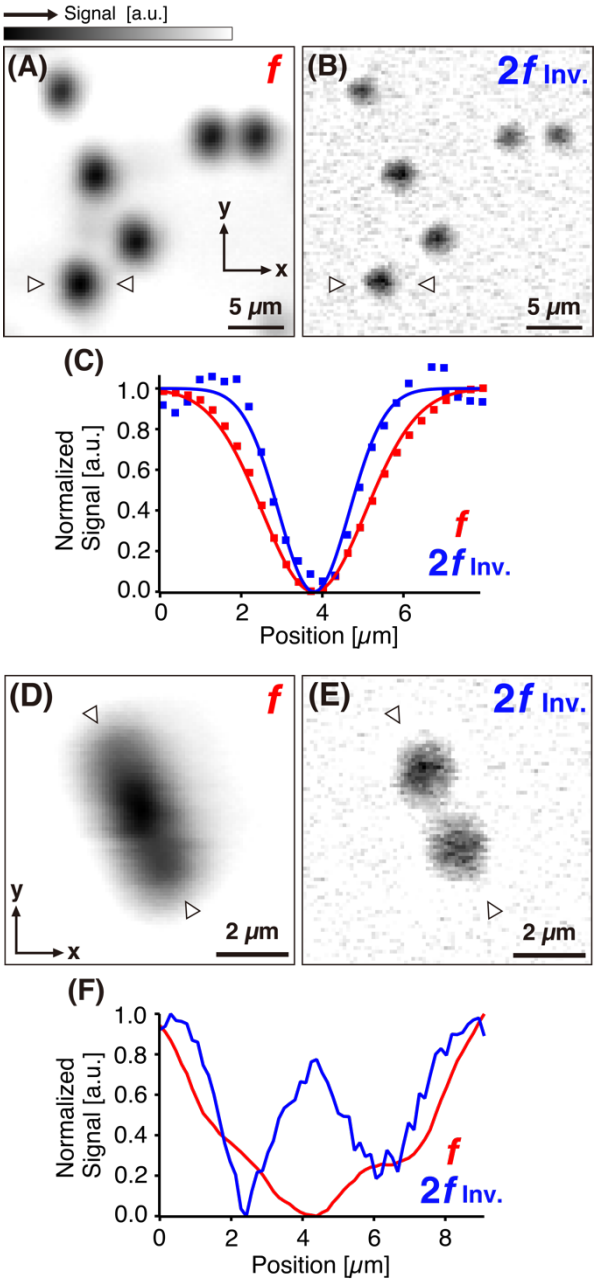

323

324 Fig. 5. (A, B) Transmission images of single polystyrene beads with a diameter of 2μm

325 stained with eosin Y, reconstructed by linear (A) and 2nd order nonlinear (B) signals. The

326 pixel size and dwell time were 303 nm and 500 μs, respectively. An objective lens with

327 an NA of 0.3 was used for illumination. (C) The line profiles of the bead images indicated

328 by white arrowheads in (A) and (B). (D, E) Transmission images of two close polystyrene

329 microbeads, reconstructed by linear (D) and 2nd order nonlinear (B) transmitted signal.
330 The pixel size and dwell time were 150 nm and 500 μs, respectively. (F) The intensity
331 profiles of bead images indicated by arrowheads in (D) and (E). The excitation intensities
332 were 56 W/cm^2 for (A, D) and 2.7×10^4 W/cm^2 for (B, E).
333
334
335 **Super-resolution transmission imaging of rat kidney tissue by SAT microscopy**
336 We demonstrated super-resolution transmission imaging of rat kidney tissue by using SAT
337 microscopy. Figures 6(A) and 6(B) show the transmission images of eosin Y-stained rat
338 kidney tissue in the focal plane (xy image), reconstructed by the linear and 2nd order
339 nonlinear signals, respectively. An objective lens with an NA of 0.3 and a magnification
340 of 10× (UMPlanFl, Olympus, Tokyo Japan) was used for the excitation, and a condenser
341 lens with an NA of 0.55 (IX2-LWUCD, Olympus, Tokyo, Japan) was used for the
342 collection of the transmitted signal. The excitation wavelength was 532 nm. The structure
343 of the renal tubule stained with eosin Y is observed in each image. In Figure 6(B), the
344 peripheries of the tissue structure were clearly identified compared to those in Figure 6(A),
345 thanks to the improvement of spatial resolution. Figures 6(C) and 6(D) are the magnified
346 images of Figures 6(A) and 6(B) at the area indicated by the orange rectangle in Figure

6(A). We obtained the line profiles indicated by the white arrowheads in Figures 6(C) and 6(D) and compared the spatial resolution in Figure 6(E). We measured the FWHMs of each signal profile by applying the Gaussian fitting. FWHMs of the profiles were 4.0 μm and 2.2 μm for Figure 6(C) and Figure 6(D), respectively. The image size of the structure was reduced about 1.8 times in Figure 6(D), which is larger than the theoretical value, which is 1.3, in Figure 2. This is due to the optical sectioning capability of SAT microscopy, which reduces the out-of-focus signals effectively. This result confirmed the improvement of the spatial resolution in the lateral direction in the image of the biological specimen.

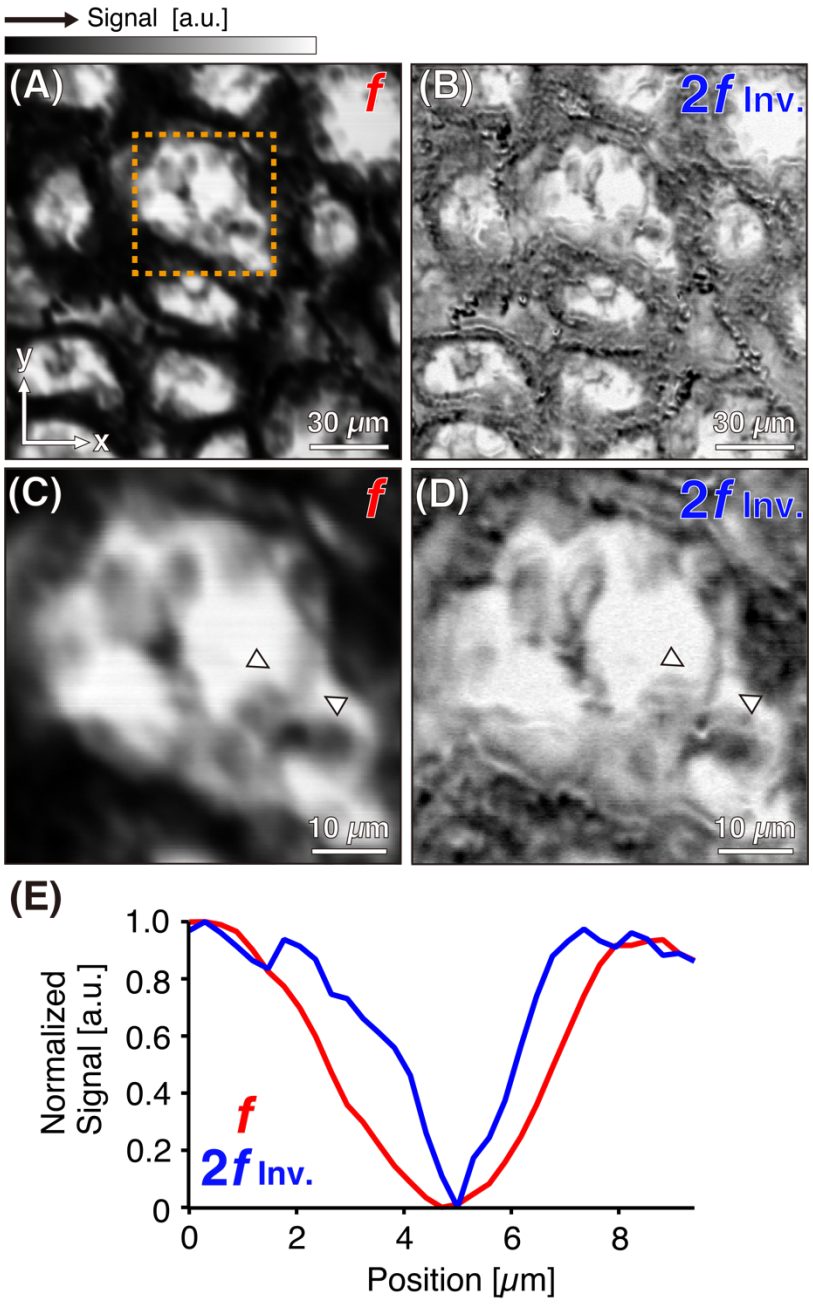

358

359 Fig. 6. (A, B) Transmission image of rat kidney tissue stained by eosin Y, reconstructed

360 by linear (A) and 2nd order nonlinear (B) signals. Excitation intensity was 1.0×10^2

361 W/cm^2 for (A) and 2.7×10^4 W/cm^2 for (B). The pixel size and dwell time were 293 nm

362 and 500 μs, respectively. An objective lens with an NA of 0.3 was used for illumination.

(C, D) Magnified images of (A) and (B) at the area indicated by the orange rectangle in (A). (E) Normalized line profiles of images indicated by white arrowheads in (C, D)

By using a high NA objective lens, we obtained a high-resolution in-plane image (xy image) of stained rat kidney tissue. We used an oil-immersion objective lens with an NA of 1.40 and a magnification of 100× (UPlanSApo, Olympus, Tokyo, Japan) for the excitation. For the collection of the transmitted signal, an oil-immersion condenser lens with an NA of 1.40 (C-AA, Nikon, Tokyo, Japan) was used. Figures 7(A) and 7(B) show the transmission images of eosin Y-stained rat kidney slice in the focal plane (xy image), reconstructed by linear and 2nd order nonlinear signals, respectively. In Figure 7(B), in addition to the improvement of the spatial resolution, the signal generated from the out-of-focus position was effectively removed by optical sectioning capability. The optical sectioning capability effectively worked for the high NA objective with a depth of focus shallower than that of a lower NA objective lens. We can confirm that the high-resolution structural information was obtained in the image reconstructed by using the nonlinear signal. These results indicate that our technique is capable of revealing finer structures in specimens than conventional transmission microscopy due to the improvement of spatial resolution and the optical sectioning capability.

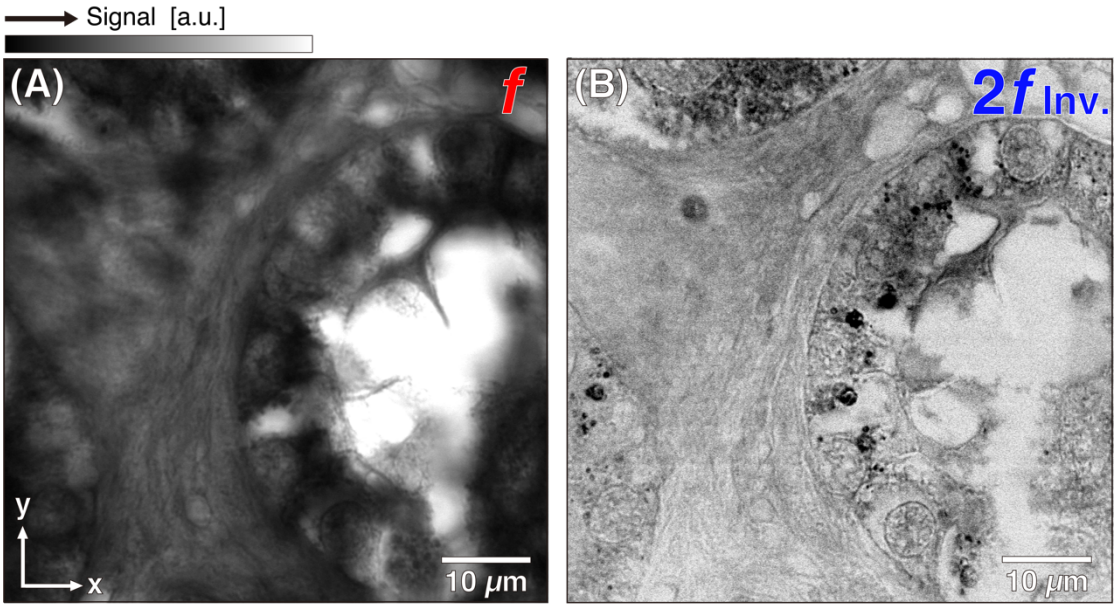

Fig. 7. (A, B) Results of high-NA (= 1.40) illumination transmission imaging of rat kidney tissue stained by eosin Y, reconstructed by linear (A) and 2nd order nonlinear (B) signals. Excitation intensities were 1.1×10^2 W/cm^2 for (A) and 1.3×10^5 W/cm^2 for (B). The pixel size and dwell time were 59 nm and 500 μs, respectively.

The use of saturated absorption can improve the spatial resolution not only in the lateral direction but also in the axial direction, as shown in our calculation in Figure 2. We demonstrated cross-sectional transmission imaging of a rat kidney tissue by using SAT microscopy to confirm the optical sectioning capability. Figure 8(A) shows a transmission in-plane image (xy image) of rat kidney tissue stained with eosin Y obtained

394 by conventional laser scanning transmission microscopy. Figure 8(B) and 8(C) show the
395 cross-sectional images (xz images) reconstructed by linear and 2nd order nonlinear
396 signals obtained at the position indicated by the dotted line in Figure 8(A). In this
397 experiment, we used an oil immersion objective with an NA of 1.40 (UPlanSApo,
398 Olympus, Tokyo, Japan) for illumination. To collect the transmitted signal from the
399 specimen, we used an oil-immersion condenser lens with an NA of 1.40 (C-AA, Nikon,
400 Tokyo, Japan). In Figure 8(B), the signals generated from the tissue layer are covered by
401 the background from out of the focus layer, and it is difficult to observe the cross-sectional
402 structure of the tissue. However, in Figure 8(C), the background signals are reduced, and
403 the morphology of the tissue layer becomes clearer, indicating the improvement of axial
404 spatial resolution by our technique. We also found that the nonlinear signals are small
405 inside the tissue layer, as indicated by solid arrows in Figure 8(C). This is probably due
406 to the high concentration of dye molecules at these locations, which causes the decrease
407 of excitation intensity and the nonlinear absorption, as discussed in Figure 3. Another
408 possible reason is the distributions of refractive index in the tissue that induce the strong
409 light scattering and prevent both excitation and collection of the signal during imaging.
410 This contrast inversion was also observed in measuring a haematoxylin-stained tissue, as
411 shown in Figure 9.

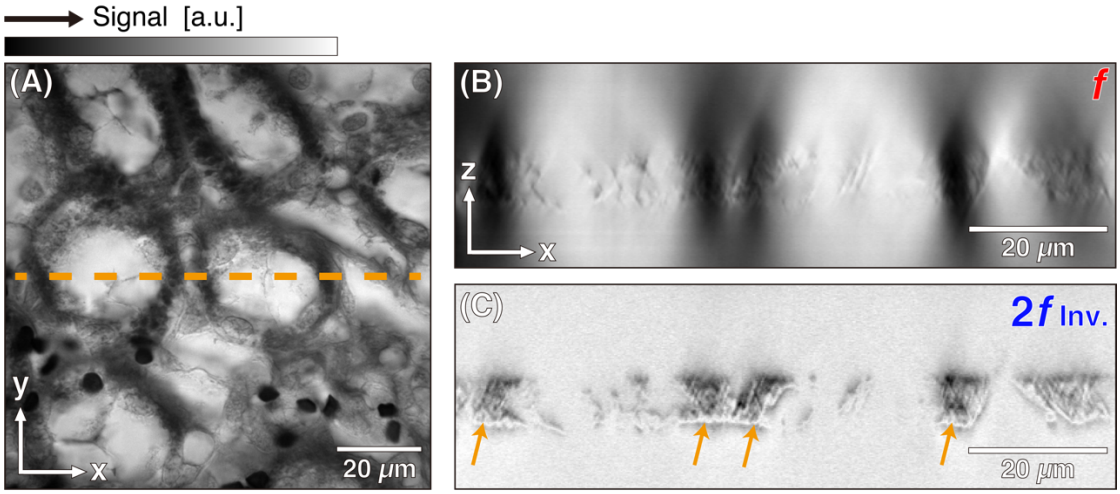

Fig. 8. (A) In-plane (xy) transmission image of rat kidney tissue stained with eosin Y, obtained by using conventional laser scanning microscopy. Excitation intensity was 3.0 $\times 10^3$ W/cm^2. The pixel size and dwell time were 195 nm and 100 μs, respectively. (B, C) Cross-sectional (xz) transmission images of rat kidney tissue obtained at the position indicated by orange dotted line in (A). (B) and (C) were reconstructed by linear and 2nd order nonlinear signals, respectively. Excitation intensities were 3.0×10^3 W/cm^2 for (B) and 1.9×10^6 W/cm^2 for (C), respectively. The pixel size and dwell time were 195 nm and 500 μs, respectively. An objective lens with an NA of 1.40 was used for illumination. The solid orange arrows in (C) indicate the locations where the image contrasts are relatively low.

Since the saturable absorption is based on the saturated excitation of the molecular state, it should be a general phenomenon that can be seen among different types of dye molecules. Thus, our technique allows us to observe the specimen stained with other dye molecules, not limited to eosin Y. Here, we demonstrated the imaging of a tissue section stained with haematoxylin, which is also one of the popular dyes in pathology.

Figures 9(A) and 9(B) show the transmission images of the haematoxylin-stained rat kidney tissue, reconstructed by linear and 2^{nd} order nonlinear signals, respectively. An objective lens with an NA of 0.3 and a magnification of 10× (UMPlanFl, Olympus, Tokyo, Japan) was used for the excitation, and a condenser lens with an NA of 0.55 (IX2-LWUCD, Olympus, Tokyo, Japan) was used for the collection of the transmitted signal. Compared to Figure 9(A), Figure 9(B) shows the distributions of the cell nuclei more clearly. Because the out-of-focus signal was suppressed by the optical sectioning capability of SAT microscopy, the image contrast was significantly improved in Figure 9(B). We obtained the line profiles of Figures 9(A) and 9(B) at the region indicated by white arrowheads in the images and compared them in Figure 9(C). In the image reconstructed by nonlinear signals (Figure 9(B)), the structures of the specimen are clearly resolved due to the improvement of spatial resolution by SAT microscopy. This result indicates that our technique allows us to use not only eosin Y but also different dye

444 molecules such as haematoxylin, as contrast probes. The observation of haematoxylin-
445 stained tissue by our technique would be useful to quantify the number of the stained cell
446 nuclei included in the tissue because our approach allows us to resolve closely located
447 cell nuclei with the improvement of three-dimensional spatial resolution. It also should
448 be noted that some structures that showed strong absorption in Figure 9(A) have lost the
449 contrast in Figure 9(B), as indicated by the orange arrows in the figures. This is
450 presumably due to the high concentration of dyes at these locations that attenuated the
451 light intensity too much to induce the nonlinear absorption that provide an image contrast
452 as discussed with our calculation in Figure 3.
453
454
455
456

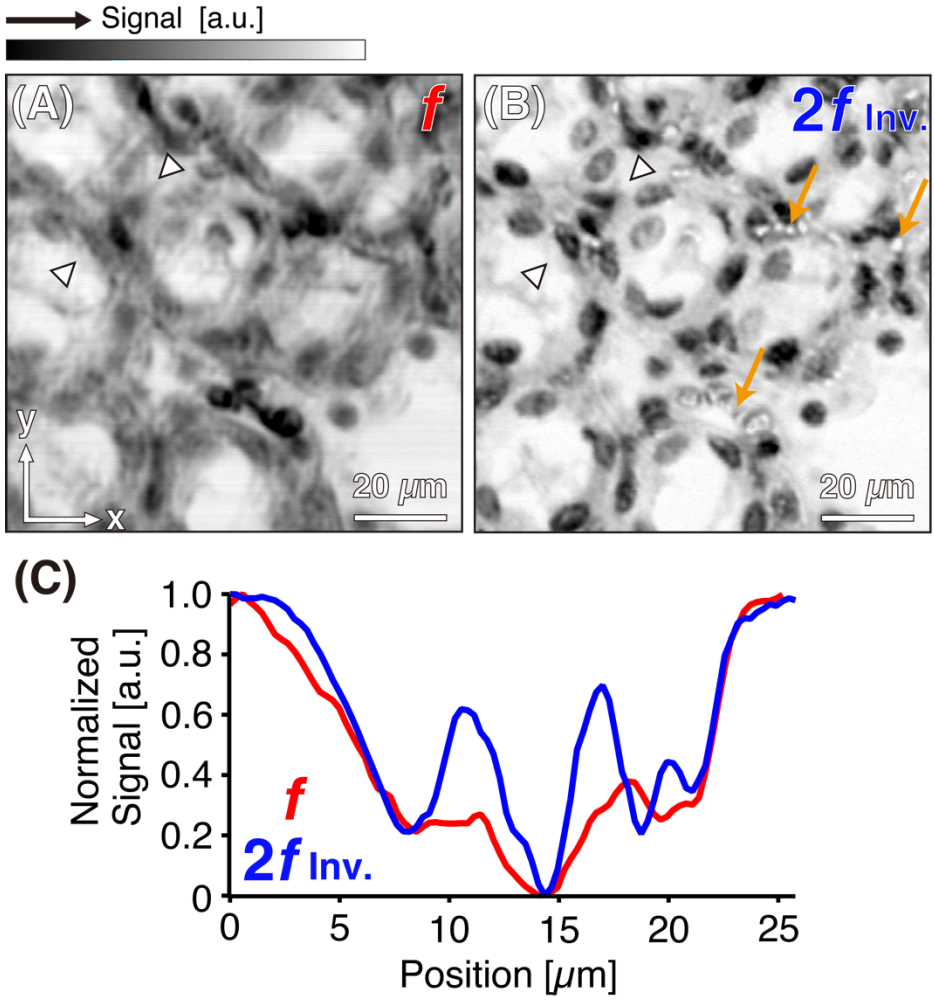

457

458

459 Fig. 9. (A, B) Haematoxylin-stained rat kidney tissue measured by transmission imaging.

460 The images were reconstructed by linear (A) and 2nd order nonlinear (B) signals,

461 respectively. Excitation intensities were 1.0×10^{2} W/cm^{2} for (A) and 4.8×10^{4} W/cm^{2} for

462 (B). The pixel size and dwell time were 293 nm and 500 μs, respectively. The solid orange

463 arrows in (C) indicate the locations where the image contrasts are relatively low. (C)

464 Normalized line profiles at the regions indicated by the white arrowheads in (A) and (B).

465

Conclusion and Discussion

In this paper, we reported a method to improve the three-dimensional spatial resolution of laser scanning transmission microscopy by exploiting the saturated absorption of dye molecules. We theoretically confirmed that absorbed light power by dye molecules is saturable at the high excitation intensity, and the nonlinear absorption signal induced in transmitted light was extracted by harmonic demodulation. The simulated images of a single point absorber indicated the improvement of three-dimensional spatial resolution in our proposed technique. We experimentally demonstrated transmission imaging of stained rat kidney section and confirmed that the structure of the specimen is clearly resolved in both lateral and axial directions by selectively detecting 2^{nd} order nonlinear signal.

In our experimental condition, the spatial resolution of SAT microscopy was 130 nm in the lateral direction, as indicated by our calculation (Figure 2). Currently, the spatial resolution of our technique has not reached that of typical fluorescence super-resolution microscopy, which achieves few tens of nanometer[30,31]. However, SAT microscopy allows us super-resolution imaging of dye-stained pathological sections prepared for the observation in conventional bright-field transmission microscopy, even without any additional treatments such as staining with fluorescence probes. This advantage can make

484 our technique a convenient and cost-effective tool for practical application in medical
485 diagnosis. The volumetric high-resolution transmission image obtained by our approach
486 would help find small lesions, which are difficult to distinguish in conventional bright-
487 field microscopy.

488 The spatial resolution in SAT microscopy can be improved further by
489 demodulating the transmitted signal at higher-order harmonic frequencies. However, the
490 signal intensity is typically lower for the higher-order nonlinear components, and it is
491 difficult to detect higher-order nonlinear signals with a signal to noise ratio (SNR) high
492 enough to visualize fine structures. In our experiment, we were not able to detect a
493 nonlinear signal higher than 3rd order. To improve the SNR in our technique, it is essential
494 to optimize the concentration of the dye molecule and the thickness of the specimen
495 properly. As indicated in our calculation results in Figure 3, the dye concentration and the
496 thickness of a specimen are the important factors for successful SAT imaging. Also,
497 photobleaching of the dye molecule is another important factor that affects the SNR of
498 our technique. Even in transmission imaging, the measurement over a long period of time
499 with high excitation intensity makes the dye molecules lose their absorption capability in
500 a similar manner to fluorescence microscopy. Using the differential excitation
501 technique[32,33] would be helpful to detect the nonlinear signal more efficiently and reduce

photobleaching in SAT imaging.

Even though the transmission images obtained by SAT microscopy provide the information of finer sample structures compared to conventional bright-field microscopy, we need to pay careful attention to interpreting the image contrast created by the nonlinear signals. As shown in our theoretical investigation shown in Figure 3, the intensity of the nonlinear transmitted signal is not always proportional to the sample thickness or dye concentration but shows more complicated behaviors, especially at the locations with strong absorbers in a sample. Moreover, in imaging of thick tissue, the amount of nonlinear transmission signals can be affected by light scattering induced by the distribution of refractive index within the sample. Because of these factors, the image contrast in the nonlinear transmission image does not always correspond to the amount of light absorption in the sample. Thus, it is necessary to find light exposure and sample preparation conditions suitable for medical diagnosis. For the same reason, the quantitative measurement of light absorption in the sample can be a challenging task for the proposed technique.

We have only shown images of specimens stained with only one of eosin Y or haematoxylin in this paper. However, the two-colour imaging for specimens stained with both eosin and haematoxylin should also be possible. For the two-colour imaging, it is

520 better to switch the excitation wavelengths between 532nm and 600 nm, which match the
521 absorption peak wavelengths of eosin Y[28] and haematoxylin[34], respectively, to make the
522 difference of the contrast between eosin Y and haematoxylin clear. The feasibility of
523 multicolour super-resolution imaging of the haematoxylin-eosin-stained specimens in our
524 technique should be investigated in our future studies.
525
526
527
528
529
530
531
532
533 **Material and Methods**
534 **Optical setup of SAT microscopy**
535 The light source was a continuous wave laser oscillating at the wavelength of 532 nm
536 (Millennia eV, Spectra-Physics, Santa Clara, California, US). The temporal modulation
537 was applied to the excitation intensity at a frequency of 10 kHz by using the interference

between diffraction beams from two acousto-optic modulators (AOM-402-AF, IntraAction, Bellwood, Illinois, US), which were driven with a difference of 10 kHz in their driving frequencies. The temporally modulated beam was focused on the sample by an objective lens. The transmitted signal through the sample was collected by using a microscope bright-field condenser lens and detected by a photomultiplier tube (H7710-13, Hamamatsu, Shizuoka, Japan). We placed a band-pass filter (FF01-534, IDEX corporation, Illinois, US) before the photomultiplier tube to selectively detect transmitted light with the same wavelength as that of excitation wavelength by blocking the fluorescence light produced from the sample. The harmonics signal included in the modulated transmitted signal was demodulated by using a lock-in amplifier (HF2LI, Zurich Instruments, Zurich, Switzerland). Two-axis galvanometer mirrors were used for the scanning of the illumination beam in the lateral directions to obtain an in-plane image of the sample. A piezoelectric translation stage was used to perform scanning in the axial direction for cross-sectional imaging.

Detection of the nonlinear transmitted signal from eosin Y solution

The transmitted signal from the eosin Y solution was detected by using a setup for SAT microscopy. The sample was commercially available 1% eosin Y solution dropped onto

a coverslip (051-0651, FUJIFILM Wako Pure Chemical Corporation, Osaka, Japan). The excitation beam was focused into the droplet of eosin Y solution by using an objective lens with an NA of 0.3 and a magnification of 10× (UMPlanFl, Olympus, Tokyo, Japan). A condenser lens with an NA of 0.55 (IX2-LWUCD, Olympus, Tokyo, Japan) was used for the collection of the transmitted signal. During the measurement of the transmitted signal, we scanned the laser spot two-dimensionally across the solution by controlling two galvanometer mirrors to avoid photo-bleaching of eosin Y.

Imaging of stained polystyrene microbeads

We stained commercial polystyrene microbeads (19814-15, Polysciences, Warrington, Pennsylvania, US; diameter = 2μm) with commercially available 1% eosin Y solution (051-0651, FUJIFILM Wako Pure Chemical Corporation, Osaka, Japan). The stained microbeads were distributed on a dried coverslip. Transmission images of the stained microbeads were obtained by using the setup of SAT microscopy. The microbeads were illuminated through an objective lens with an NA of 0.3 and a magnification of 10× (UMPlanFl, Olympus, Tokyo, Japan). The excitation wavelength was 532 nm. The transmitted signal was collected by using a condenser lens with an NA of 0.55 (IX2-LWUCD, Olympus, Tokyo, Japan).

574

575 **Preparation of stained rat kidney tissue**

576 The kidney tissue was excised from an adult male Sprague-Dawley rat at 30 weeks old
577 under anesthesia, then was cut into a thickness of 5 mm after being washed with
578 phosphate-buffered saline (PBS). After the organ was harvested, euthanasia was
579 immediately applied to the rat. The sliced kidney was fixed with immersion in 10%
580 formalin solution overnight and dehydrated with ethanol. After replacing ethanol with
581 xylene, the tissue was embedded in paraffin by immersing the 1:1 mixture of xylene and
582 paraffin overnight at 40–50 ºC, and for three hours at 60-65 ºC, consecutively. The
583 paraffin-embedded kidney tissue was sliced into a thickness of 3 μm by using a
584 microtome and expanded onto a slide glass. The thin paraffin section was deparaffinized
585 with xylene and ethanol and stained by immersing in dye solution at the concentration of
586 4 mM for 2 minutes. After the dehydrating and permeating operation by using ethanol
587 and xylene, the slice was sealed by a coverslip with the addition of a mounting medium.
588 All animal experiments were conducted with the approval of and following guidelines
589 from the Animal Research Committee of Kyoto Prefectural University of Medicine.

590

591

Acknowledgment

This work was supported by JST CREST Grant No. JPMJCR15N3, Japan. The authors thank T. Kubo of Osaka University for his valuable advice.

References

1. Wilson, T., (1986) Confocal Light Microscopy, Ann. N. Y. Acad. Sci. 483, 416-427.
2. Wilson, T., (1990) Confocal Microscopy, Academic Press, California
3. Kino, G.S., Corle, T.R., (1996) Confocal Scanning Optical Microscopy and Related Imaging Systems. Academic Press, California.
4. Corle, T.R., Chou, C.-H., Kino, G.S., (1986) Depth response of confocal optical microscopes, Opt. Lett. 11, 770–772.
5. Sheppard, C.J.R., Gu, M., Mao, X.Q., (1991) Three-dimensional coherent transfer function in a reflection-mode confocal scanning microscope, Opt. Commun. 81, 281–284.
6. Brakenhoff, G.J., Van Der Voort, H.T.M., Van Spronsen, E.A., Linnemans, W.A.M., Nanninga, N., (1985) Three-dimensional chromatin distribution in

neuroblastoma nuclei shown by confocal scanning laser microscopy, Nature 317, 748–749.

7. White, J.G., Amos, W.B., Fordham, M., (1987) An evaluation of confocal versus conventional imaging of biological structures by fluorescence light microscopy., J. Cell Biol. 105, 41–48.

8. Nakamura, O., Kawata, S., (1990) Three-dimensional transfer-function analysis of the tomographic capability of a confocal fluorescence microscope, J. Opt. Soc. Am. A 7, 522–526.

9. Carlsson, K., Danielsson, P.E., Liljeborg, A., Majlöf, L., Lenz, R., Åslund, N., (1985) Three-dimensional microscopy using a confocal laser scanning microscope, Opt. Lett. 10, 53-55.

10. Sheppard, C.J.R., Mao, X.Q., (1989) Three-dimensional imaging in a microscope, J. Opt. Soc. Am. A 6, 1260–1269.

11. Tian, P., Warren, W.S., (2002) Ultrafast measurement of two-photon absorption by loss modulation, Opt. Lett. 27, 1634-1636.

12. Fischer, M.C., Ye, T., Yurtsever, G., Miller, A., Ciocca, M., Wagner, W., Warren, W.S., (2005) Two-photon absorption and self-phase modulation measurements with shaped femtosecond laser pulses, Opt. Lett. 30, 1551-1553

628 13. Sasaki, K., Koshioka, M., Masuhara, H., (1992) Confocal laser-induced absorption
629 microscope, J. Opt. Soc. Am. A 9, 932–936.
630 14. Tong, L., Liu, Y., Dolash, B.D., Jung, Y., Slipchenko, M.N., Bergstrom, D.E.,
631 Cheng, J.X., (2012) Label-free imaging of semiconducting and metallic carbon
632 nanotubes in cells and mice using transient absorption microscopy, Nat.
633 Nanotechnol. 7, 56–61.
634 15. Chen, T., Lu, F., Streets, A.M., Fei, P., Quan, J., Huang, Y., (2013) Optical
635 imaging of non-fluorescent nanodiamonds in live cells using transient absorption
636 microscopy, Nanoscale 5, 4701–4705.
637 16. Ye, T., Fu, D., Warren, W.S., (2009) Nonlinear absorption microscopy, Photochem.
638 Photobiol. 85, 631–645.
639 17. Fischer, M.C., Wilson, J.W., Robles, F.E., Warren, W.S., (2016) Invited Review
640 Article: Pump-probe microscopy, Rev. Sci. Instrum. 87, 031101.
641 18. Fu, D., Ye, T., Matthews, T.E., Chen, B.J., Yurtserver, G., Warren, W.S., (2007)
642 High-resolution in vivo imaging of blood vessels without labeling, Opt. Lett. 32,
643 2641–2643.
644 19. Tokeshi, M., Uchida, M., Hibara, A., Sawada, T., Kitamori, T., (2001)
645 Determination of subyoctomole amounts of nonfluorescent molecules using a

646 thermal lens microscope: Subsingle-molecule determination, Anal. Chem. 73,
647 2112–2116.
648 20. Boyer, D., Tamarat, P., Maali, A., Lounis, B., Orrit, M., (2002) Photothermal
649 imaging of nanometer-sized metal particles among scatterers, Science (80-.). 297,
650 1160–1163.
651 21. Min, W., Lu, S., Chong, S., Roy, R., Holtom, G.R., Sunney Xie, X., (2009)
652 Imaging chromophores with undetectable fluorescence by stimulated emission
653 microscopy, Nature 461, 1105–1109.
654 22. Milonni, P., Eberly, J., (1988) Lasers, A Wiley-Interscience publication, New
655 York.
656 23. Svelto, O., (1976) Principles of lasers, Plenum Press, New York.
657 24. Danielli, A., Maslov, K.I., Garcia-Uribe, A., Winkler, A.M., Li, C., Wang, L.,
658 Chen, Y., Dorn, G.W., Wang, L. V., (2014) Label-free photoacoustic nanoscopy,
659 J. Biomed. Opt. 19, 086006.
660 25. Fujita, K., Kobayashi, M., Kawano, S., Yamanaka, M., Kawata, S., (2007) High-
661 resolution confocal microscopy by saturated excitation of fluorescence, Phys. Rev.
662 Lett. 99, 228105.
663 26. Yamanaka, M., Yonemaru, Y., Kawano, S., Uegaki, K., Smith, N.I., Kawata, S.,

Fujita, K., (2013) Saturated excitation microscopy for sub-diffraction-limited imaging of cell clusters, J. Biomed. Opt. 18, 126002.

27. Jones, G., Farahat, C.W., Oh, C., (1994) Photoinduced electron transfer involving eosin-tryptophan conjugates. long-lived radical pair states for systems incorporating aromatic amino acid side chains, J. Phys. Chem. 98, 6906–6909.

28. Jones, G.R., Duddell, A. D., Murray, D., Cundall, R. B., Catterall, R.,(1984) Eosin Y-macromolecule complexes. Part 1. - Application of exciton theory to the study of the arrangement of eosin Y molecules in polycation-induced eosin Y dimers, J. Chem. Soc., Faraday Trans. 2 80, 1181–1199.

29. Lee, H., Oketani, R., Huang, Y.-T., Li, K.-Y., Yonemaru, Y., Yamanaka, M., Kawata, S., Fujita, K., Chu, S.-W., (2014) Point spread function analysis with saturable and reverse saturable scattering, Opt. Express 22, 26016-26022.

30. Leung, B.O., Chou, K.C., (2011) Review of super - resolution fluorescence microscopy for biology, Appl. Spectrosc. 65, 967–980.

31. Vangindertael, J., Camacho, R., Sempels, W., Mizuno, H., Dedecker, P., Janssen, K.P.F., (2018) An introduction to optical super-resolution microscopy for the adventurous biologist, Methods Appl. Fluoresc. 6, 022003.

32. Nawa, Y., Yonemaru, Y., Kasai, A., Oketani, R., Hashimoto, H., Smith, N.I., Fujita,

K., (2018) Saturated excitation microscopy using differential excitation for efficient detection of nonlinear fluorescence signals, APL Photonics 3, 080805.

33. Oketani, R., Doi, A., Smith, N.I., Nawa, Y., Kawata, S., Fujita, K., (2017) Saturated two-photon excitation fluorescence microscopy with core-ring illumination, Opt. Lett. 42, 571–574.

34. Kmetz, J.M., Gallagher, M.S., Anthony, A., (1967) Spectral analysis of hematoxylin in tissue sections, Proc. Pennsylvania Acad. Sci. 41, 177–181.